

# Threaded Versus Porous-Surfaced Implants as Anchorage Units for Orthodontic Treatment: Three-dimensional Finite Element Analysis of Peri-implant Bone Tissue Stresses

Robert M. Pilliar, BSc, PhD<sup>1</sup>/Genadijs Sagals, MSc, PhD<sup>2</sup>/Shaker A. Meguid, BSc, MSc, PhD<sup>3</sup>/  
Rodrigo Oyonarte, DDS, MSc-Ortho<sup>4</sup>/Douglas A. Deporter, DDS, PhD<sup>5</sup>

**Purpose:** A 3-dimensional finite element model was developed to investigate the cause of different crestal bone loss patterns observed around sintered porous-surfaced and machined (turned) threaded dental implants used for orthodontic anchorage in a previously reported animal study. **Materials and Methods:** Twenty-noded structural solid elements with parabolic interpolation between nodes were used for modeling the bone-implant interface zone. A 3-N traction force acting between either 2 porous-surfaced or 2 machined threaded implants placed in canine premolar mandibular sites and bone profiles observed at initiation and 22 weeks of orthodontic loading were modeled. **Results:** Higher maximum stresses in peri-implant bone next to the coronal region of the implants were predicted with the machined threaded implants at both the initial and final time points, with the values 20% greater than those predicted after the 22-week loading period. These values were approximately 200% greater than those predicted for the porous-surfaced implants, for which a more uniform stress distribution was predicted. **Discussion:** The finite element model results indicated that the observed greater retention of crestal bone next to the porous-surfaced implants was attributable to lower peak stresses developing in crestal peri-implant bone with this design, which decreased the probability of bone loss related to local overstressing and bone microfracture. **Conclusion:** The predicted lower stresses were a result of the more uniform transfer of force from implant to bone with the porous-surfaced implants, which was a consequence of the interlocking of bone and implant possible with this design. INT J ORAL MAXILLOFAC IMPLANTS 2006;21:879-889

**Key words:** crestal bone loss, finite element analysis, implant surfaces

The use of osseointegrated dental implants as anchorage units for orthodontic procedures offers advantages in complex cases and eliminates the need for extraoral sources of anchorage such as headgear.<sup>1,2</sup> Essential for success of this approach is the assurance of adequate implant stability for the

period for which orthodontic force application is needed. Threaded commercially pure titanium implants meant to be removed following completion of orthodontic treatment, including special mini-implant designs with diameters < 2 mm, have been used for such procedures with successful outcomes,<sup>3,4</sup> but on occasion they do loosen and fail before completion of treatment. To date, implants placed for use as orthodontic anchorage units have been limited to machined (turned) threaded designs with or without surface modifications.<sup>5-8</sup> Long implant length and the availability of suitable bone into which the implant can be placed (ie, dense bone with adequate blood supply and sufficient bone height to accept the implants) are prerequisites for the successful use of threaded implants. Threaded mini-implants, for example, have been recommended for use in lengths of 9 to 15 mm<sup>9</sup>; however, such long lengths do increase the risk of damage to adjacent tooth roots or vital structures.

<sup>1</sup>Professor, Faculty of Dentistry, and Institute of Biomaterials and Biomedical Engineering, University of Toronto, Canada.

<sup>2</sup>Research Associate, Department of Mechanical and Industrial Engineering, University of Toronto, Canada.

<sup>3</sup>Professor, Department of Mechanical and Industrial Engineering, University of Toronto, Canada.

<sup>4</sup>Assistant Professor, Faculty of Dentistry, Universidad de los Andes, Santiago, Chile.

<sup>5</sup>Professor, Faculty of Dentistry, University of Toronto, Canada.

**Correspondence to:** Dr Robert M. Pilliar, Faculty of Dentistry, University of Toronto, 124 Edward Street, Toronto, ON M5G 1G6, Canada. Fax: +416 979 4760. E-mail: bob.pilliar@utoronto.ca

Endosseous dental implants with a sintered porous surface structure and a press-fit design have been used successfully for conventional dental implantation for more than 15 years.<sup>10,11</sup> The 3-dimensional interconnected porous network forming the surface region of such implants allows implant fixation by bone ingrowth and can result in effective anchorage. As a result, successful osseointegration of very short implants ( $\leq 7$  mm) is possible.<sup>12-14</sup> Endopore implants (Innova, Toronto, ON, Canada) are porous-surfaced implants made of Ti-6Al-4V alloy. The porous surface layer is approximately 0.3 mm thick and is prepared by sintering Ti-6Al-4V alloy powders over a machined titanium alloy core to form a structure with approximately 35% of its volume consisting of interconnected pores.<sup>15</sup> The resulting open-pored structure (average pore size about 75 to 100  $\mu\text{m}$ ) is suitable for virtually uninhibited bone ingrowth and gives secure implant-to-bone fixation.

Conventional use of implants of this design for tooth replacement has demonstrated that the required initial stability can be achieved using press-fit placement techniques; in fact, successful outcomes can be achieved with shorter implants than are normally used with other threaded or press-fit designs.<sup>15</sup> The porous surface structure has been shown to be osteoconductive<sup>16</sup> and to result in faster osseointegration compared with plasma-sprayed implants.<sup>17</sup> The former characteristic is believed to be related to the surface features of the porous sintered region, while the latter appears to be due to the establishment of a more osteogenic stress state at the implant-bone interface in accordance with Carter's tissue differentiation hypothesis,<sup>18</sup> as shown in a finite element analysis (FEA) by Simmons and colleagues.<sup>19</sup> This, as well as the additional benefits of efficient implant fixation and long-term stability resulting from the 3-dimensional (3D) interlock of bone within this region, suggested the possible use of porous-surfaced implants as orthodontic anchorage units.

An animal study using dogs was undertaken to explore this possibility. The results of that study were encouraging and have been reported elsewhere.<sup>20,21</sup> An interesting observation in that study was the significantly different peri-implant bone loss that developed over the 24-week implantation period for machined (turned) threaded versus sintered porous-surfaced implants, with significantly greater crestal bone loss observed next to the machined implants.

Development and maintenance of rigid implant fixation during a period of orthodontic loading is essential for effective treatment. Secure fixation can be compromised by significant peri-implant bone

loss. Crestal peri-implant bone loss can be the result of a number of factors, including biomechanical factors: high localized stresses can cause bone microfracture and subsequent resorption, while abnormally low stresses related to implant-related stress protection can lead to disuse atrophy.

To determine whether the difference between machined threaded and sintered porous-surfaced implant designs might have resulted in significant differences in peri-implant stresses that could have caused the different bone loss patterns observed in earlier studies,<sup>20,21</sup> an FE model of the orthodontic loading used in that research was developed, and peri-implant stresses and strains for the model were determined. It was hypothesized that a more uniform distribution of stresses would be predicted next to porous-surfaced implants because of the ability for more effective tensile force transfer across the implant-bone junction with this design, a consequence of the 3D interlocking at the bone-implant interface. This, in turn, would be expected to reduce maximum local stresses, thereby reducing the probability of crestal bone loss caused by overloading.

## MATERIALS AND METHODS

### Model Development

In the animal study reported by Oyonarte and associates,<sup>20,21</sup> an orthodontic traction force of about 3 N (300 grams) was applied between 2 implants placed on either side of the dog mandible. Pairs of implants of 1 design or the other were placed in healed extraction sites created by removing the mandibular second, third, and fourth premolars and first molars. The implants were kept buried and out of function for a 6-week period during which all the implants became osseointegrated. Two additional control implants were also implanted, 1 on either side of the mandible, in more distal positions. Orthodontic traction was not applied to these control implants; however, they were not relevant to the objective of the FE study. At 6 weeks, 6-mm-long transgingival abutments were connected to the implants, and 1 week later, a nickel-titanium coil spring was fitted to these to apply a traction force between each pair of orthodontically loaded implants. A force of 100 grams was applied for the next 5 weeks and then replaced with a heavier coil spring to give a traction force of 300 grams, which was maintained for the next 17 weeks.

Table 1 and Figs 1a and 1b summarize the implant and abutment dimensions used in the animal experiment and modeled in the FEA. During the period of implant-related healing (6 + 1 weeks) and then during orthodontic loading (5 + 17 weeks), some crestal

bone loss occurred, so that by the end of the study, the position of the bone crest had changed. Figs 2a and 2b are representations of the average final bone configuration as reported by Oyonarte and associates.<sup>20</sup> The initial and final geometries were modeled; the major focus was determination of differences in the peri-implant bone tissue stresses between the 2 designs. The common 2D simplifications (plane stress/strain and axisymmetry) were considered inappropriate for accurately describing the bone and implant geometry and loading conditions. Therefore, a full 3D FEA was employed in the current research. A number of simplifying assumptions were made. The bone was treated as an isotropic linear elastic homogenous material, and the presence of cortical peri-implant bone only was assumed. Furthermore, any superimposed axial loads that may have resulted from the animals inadvertently loading their abutments during chewing of food or other items were ignored. Since only the difference between implant

designs was of interest, these assumptions seemed acceptable. Prediction of the absolute levels of bone tissue stress or strain was not attempted.

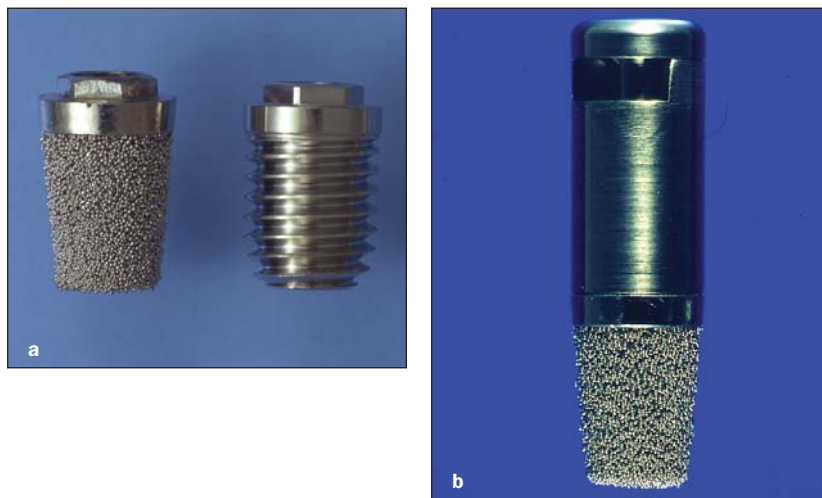
A significant finding from a preliminary 2D FE study undertaken to determine conditions for the 3D

**Table 1** Details of Geometry Used in FE Models

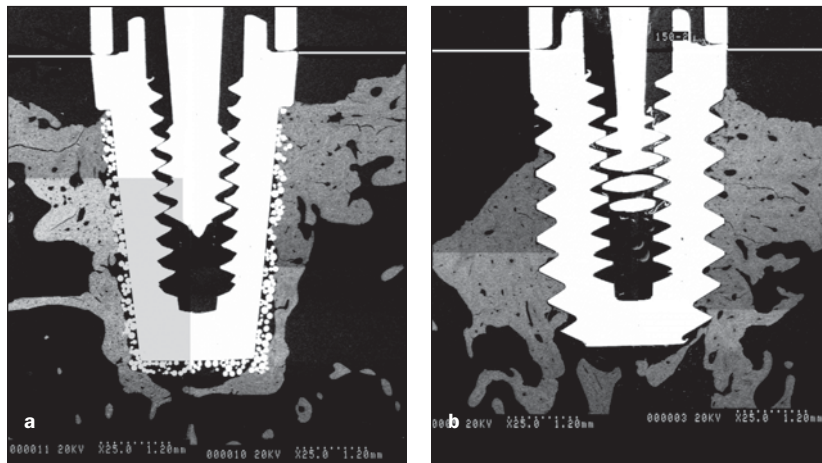
Description	Value
Implant radius (r)	2.05 mm
Distance between 2 implants (2a)	15.5 mm
Total bone depth (h <sub>1</sub> )	5 mm—initial value 4 mm—final value
Distance from the applied force level to the bone surface (h <sub>2</sub> )	6 mm
Distance from the implant centerline to the fixed bone boundary (L)	7.41 mm
No. of threads	8
Thread pitch (h)	0.6 mm
Thread angle (α)	60 degrees

**Fig 1a** (left) Porous-surfaced and (right) machined threaded implant components.

**Fig 1b** Abutment affixed to a porous-surfaced implant.



**Fig 2** Typical back-scattered scanning electron microscopic (SEM) images of anchorage implants obtained after the 22-week period of orthodontic force application (traction force application to the left) of (a) a porous-surfaced implant (note the bone retained next to the sintered porous region) and (b) a machined threaded implant showing bone loss next to the most coronal threaded region.



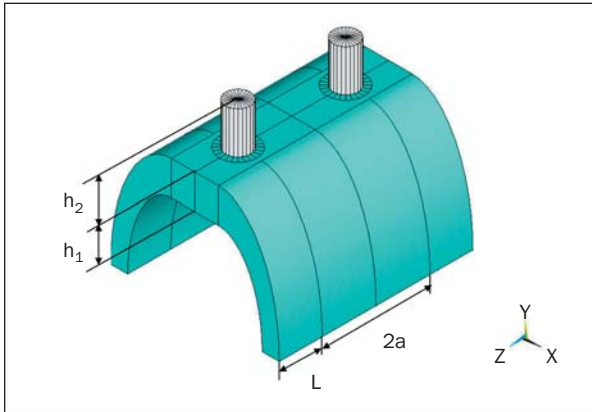


**Fig 3 (Left)** 3D model of experimental setup.

**Fig 4 (Upper right)** 3D FE model of the machined threaded implant (one quarter of a full model). (a) Full view of the mesio-distal section and (b) enlarged view of the implant area.

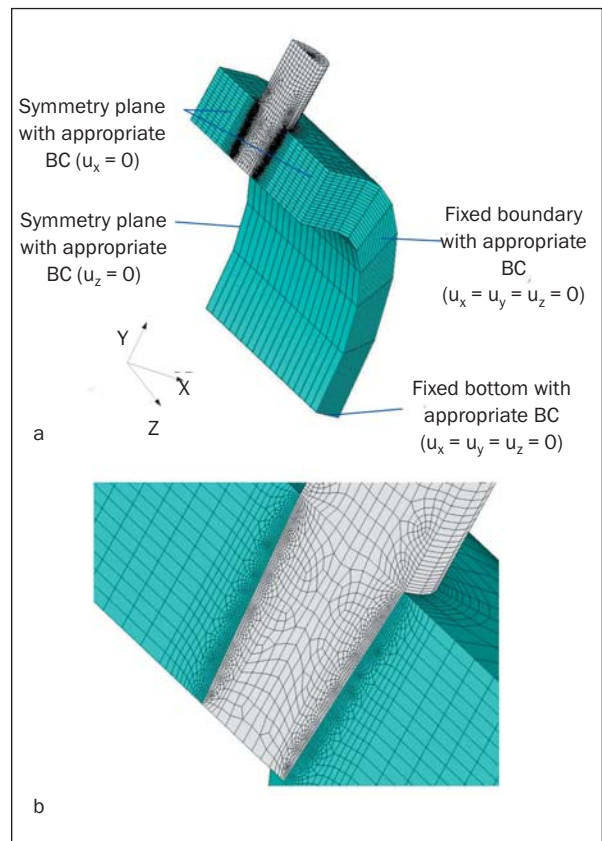
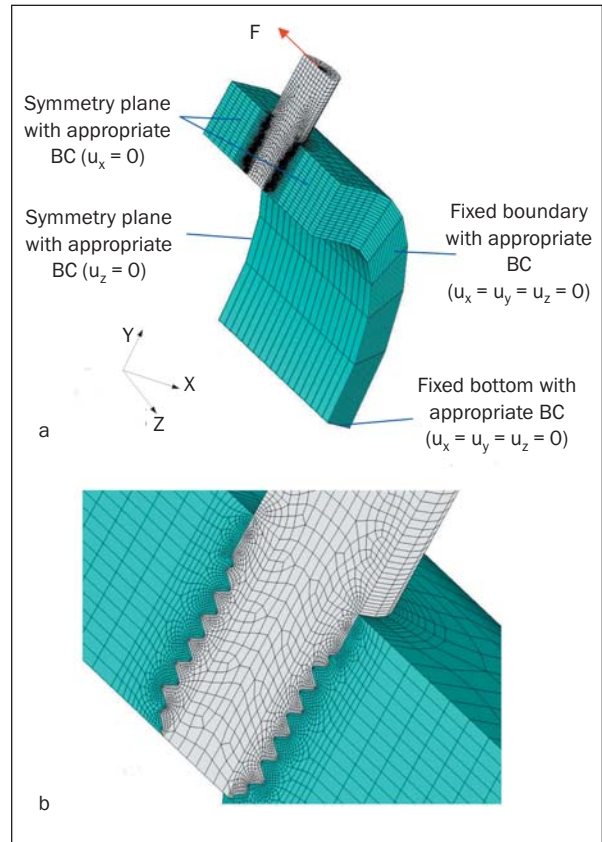
**Fig 5 (Bottom right)** 3D FE model of the porous-surfaced implant (one quarter of a full model). (a) Full view of the mesio-distal section and (b) enlarged view of the implant area.

modeling was the importance of selecting a refined mesh with appropriate element geometry within the bone-implant interface zone to capture any high local stress/strain effects in this region. Others have also noted the importance of mesh refinement for properly studying peri-implant effects.<sup>22</sup> Accordingly, the 3D models used in the present study included a refined mesh within this region. This refined mesh consisted of 20-noded 3D structurally solid elements with parabolic interpolation between nodes and was used for modeling both the implant and the bone close to the interface. A full 3D FEA was employed using the commercial code ANSYS (version 5.6 and higher, Canonsburg, PA). The full 3D model is shown in Fig 3. Because of symmetry, only 1 quarter of this full model was considered discretely, with appropriate boundary conditions, as shown in Figs 4 and 5. This allowed a considerable reduction in the size of the FE model without compromising the model accuracy.

The boundary conditions used were as follows:

- The inferior bone-implant interface was rigidly fixed.
- Out-of-plane components of bone displacement in the plane of symmetry between the 2 implants were not allowed.
- Out-of-plane components of bone displacement in other planes of symmetry passing through the center line of the implants also were not allowed.

The line of orthodontic traction was set parallel to the mesial-distal midline.



To properly model the interactions between implant and bone, contact surfaces were created at the implant and bone surfaces where bone-implant contact was anticipated following osseointegration (initially and at the termination of the loading period). In the animal study, the implants were initially positioned with the superior surface of the implant flush with the crestal bone surface (or as nearly so as possible). A surface-to-surface contact algorithm and combined penalty and Lagrange multiplier method was used to enforce appropriate boundary conditions at these surfaces.<sup>23</sup>

Because of bone ingrowth into the porous-surfaced implant region (ie, the apical 4 mm of the 5-mm-long implant), contact surfaces were created on the coronal 1 mm of the machined implant surface and on the juxtaposed bone surface only. Complete bonding was assumed along the apical 4-mm-long porous-surfaced region, since it is known that as a result of bone ingrowth into the 3D interconnected network of pores, a strongly bonded junction resistant to tensile as well as shear and compressive interface forces is formed. In order to demonstrate the appropriateness of this complete-bonding assumption, submodeling of a portion of the interface zone in the region in which maximum stress and strain were predicted using the simpler complete-bonding model was undertaken. Submodeling is a finite element technique used to get more accurate results in a region of the model of special interest. In this study, a submodeling technique available in ANSYS was used<sup>24</sup> to model implant fixation by mechanical interlocking of bone and the porous layer. The significance of the submodel on predicted peri-implant stresses in comparison to the complete-bonding model was determined.

For the machined implants, contact surfaces were created along the entire implant-bone interface. This simulated the properties of this interface, with zero resistance to tensile forces acting at the interface.

Frictionless contact was assumed for all the FE models examined. This assumption was based on the following:

- While some values of friction acting at the bone-implant interface have been reported,<sup>25</sup> there is still uncertainty about these values.
- The effect of friction upon the stress/strain distribution in both the bone and implant should be limited, since the interface contact loading was assumed to be primarily normal to the interface for both designs.

In addition, the results of preliminary 2D FEA assuming either very high ( $\mu_f = 1$ ) or negligible ( $\mu_f = 0.01$ ) values of coefficient of friction showed a negli-

**Table 2 Elastic Properties of the Materials Used in FE Models**

Material	E (GPa)	$\nu$
Ti-6Al-4V (implant)	110	0.33
Cortical bone	15	0.3

E = Young's modulus,  $\nu$  = Poisson's ratio.

gible effect of friction (< 1%) on predicted peri-implant stresses and strains for the porous-surfaced implant and a limited effect (< 10%) for the machined threaded implant design.

The main dimensions of the FE models for the 3D model reported here are shown in Table 1 and Fig 3. The distance from the implant axis to the fixed bone boundary,  $L = 7.41$  mm (see Fig 3), was similar to that used previously by Vaillancourt and associates.<sup>26</sup> The orthodontic traction force  $F$  between the implants was modeled as a 3-N force acting as a point load through the axes of the implants (Figs 3 to 5). While the properties of the bone and implant were assumed to be linear elastic and isotropic (Table 2), the FE models implemented were nonlinear because of the presence of implant-bone contact and interfacial stresses. The 0.3-mm-thick porous region with its ingrown bone was not modeled separately, as was done in other studies,<sup>19,26</sup> since its properties were not well defined. However, it is important to note that without this layer, the model represents an extreme case, with maximum stress/strain values inside the bone. Other studies have shown that the inclusion of a porous region with its ingrown bone in an FE model leads to a significant decrease in these maximum values.<sup>26</sup> Therefore, the model used in the present study for the porous-surfaced implant design is conservative in terms of demonstrating benefits related to reduced bone stresses next to the most coronal region of implants prepared with a sintered porous layer.

Two different cases were examined for each implant design. They corresponded to initial and final bone height configurations with crestal bone height ( $h_1 = 5$  mm) for the initial state and a reduced crestal bone height ( $h_1 = 4$  mm) for the final state. Evaluation of these 2 cases provided a prediction of peri-implant stresses assuming progressive bone loss resulting during implant loading (as observed in the animal experiment) and insight into a possible biomechanical causative effect.

### Submodel Development

Figures 6a and 6b show the layout for the proposed submodel inside the full FE model and an enlarged view of the submodel, respectively. The region of fine modeling inside the proposed submodel had 16 interconnecting (sintered) titanium-alloy particles and

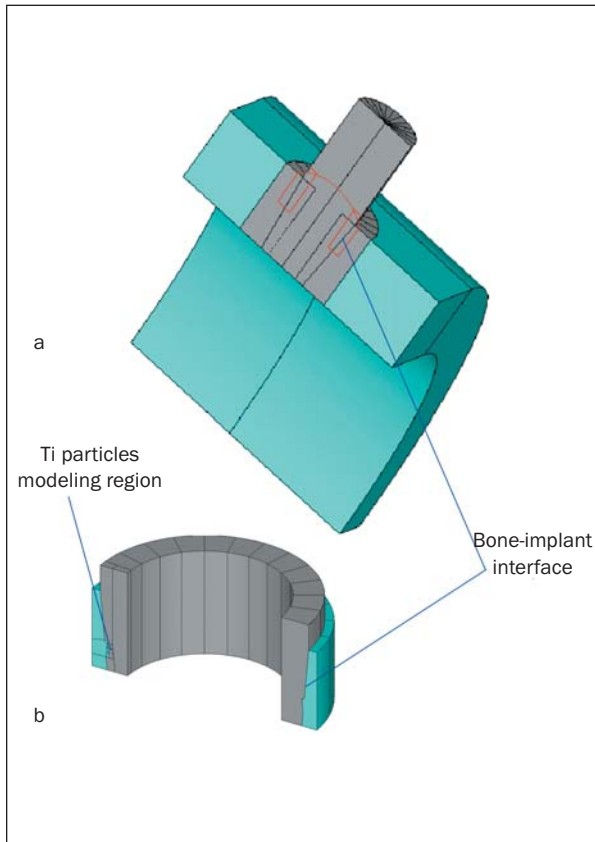


**Fig 6** (a) The layout for the proposed submodel inside the full FE model and (b) an enlarged view of the submodel.

ingrown bone. The rest of the submodel was assumed to have perfect bone-implant bonding similar to the complete bonding model. Due to symmetry, only one half of the submodel was analyzed. The titanium-alloy particles were assumed to be interconnected spheres of equal size, and the “sinter neck” diameters were assumed to be equal to 0.3 times the particle radius (Fig 7). The sphere radius, sinter neck radius, and volume percent porosity of this submodel were based on experimental measurements.<sup>11</sup> Figure 8 illustrates the FE discretization for the entire submodel and the enlarged view of the region with the maximum bone stress/strain values. Due to the complicated geometry, FE meshing in the bone ingrowth region was conducted using 3D structural solid elements (tetrahedrons) with 10 nodes with parabolic interpolation instead of solid brick elements with 20 nodes. However, the much higher mesh density in this region provided even higher accuracy for the FE results compared with the entire model. The rest of the submodel was made discrete using the prism option of the brick elements, with the sizes in the circumferential direction similar to those used in the complete-bonding model. To model the implant-bone interaction inside

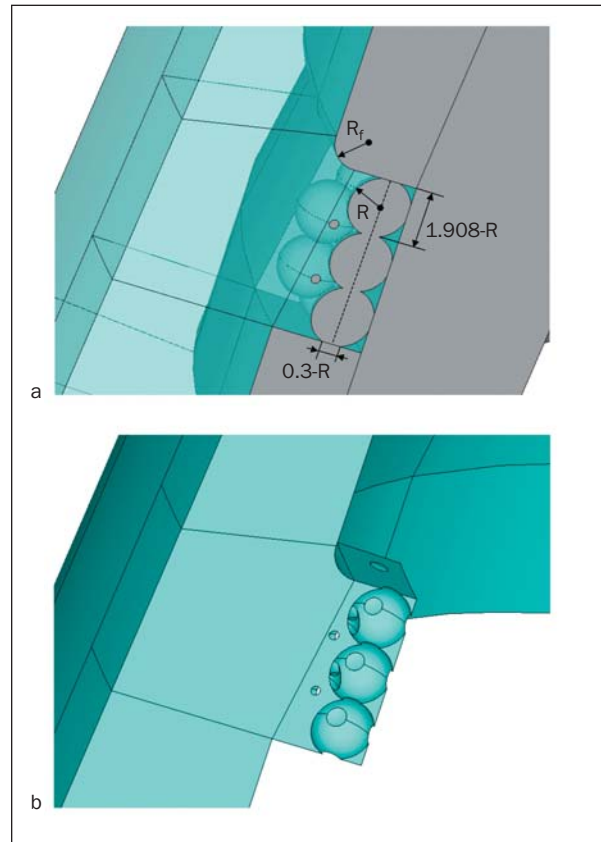


**Fig 7** Enlarged view of the bone ingrowth region. (a) Titanium (dark regions) and bone (light regions) can be seen. (b) Bone only.

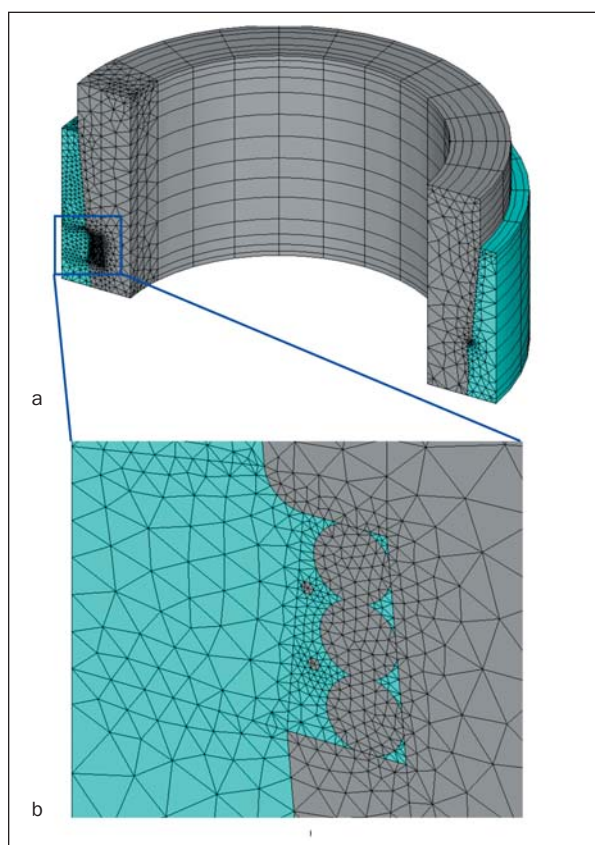
the bone ingrowth region, frictionless contact elements were created at all interfaces within this region.

## RESULTS

### FEA—Complete Bonding Model

The results of the 3D FEA, assuming complete bonding at the bone/porous surface interface, are summarized in Table 3, with the maximum values of the equivalent von Mises stress and strain shown for the initial and final bone height configurations. The analysis predicted considerably higher maximum stresses for the machined threaded implant design compared with the porous-surfaced design, particularly for the final bone configuration case.

To show the stress distribution along the bone-implant interface in both the superior-to-inferior and mesial-distal directions, the equivalent von Mises stresses in bone along 2 interface lines, 1 at the bone-implant interface at the buccal-lingual mid-plane section of the implant and along its length (Fig 9) and the other at the interface and along the implant circumference at a depth of 1 mm below the initial

**Table 3 FEA Results**

	Maximum Von Mises stress (MPa) Bone position		Maximum Von Mises microstrain Bone position	
	Initial	Final	Initial	Final
Machined threaded implant	6.56	8.03	569	696
Porous-surfaced implant	4.02	4.00	349	346

**Fig 8** (Left) FE discretization of the submodel: (a) the entire submodel and (b) an enlarged view of the fine modeled bone ingrowth region with maximum bone stress/strain values.

bone surface (Fig 10) were calculated and plotted. The selection of the location of these lines was governed by the location of the maximum values of von Mises stress. The “depth” on these plots (abscissa in Figs 9a and 9b) represents the vertical distance from the initial crestal bone surface position. Figure 10 shows the von Mises stress distribution at the interface along the circumference at the depth where these stresses reach their maximum values. The 0-degree position corresponds to the bone next to the implant surface in the direction of the traction force (the compression side), while the 180-degree position is bone at the diametrically opposite “tension” side. These plots show clearly the more uniform stress distribution at the bone-implant interface at this level with the porous-surfaced design.

For the machined threaded implant design, the maximum equivalent stress occurred at the tip of the most coronal thread on the side of the implant in which crestal bone was in compression (ie, downstream from the traction force). The development of high stresses in this region was expected because of the implant tipping caused by the traction force. A high stress zone can also be noted at the apical region

of the implant next to the diametrically opposite implant surface. In both of these regions, high compressive stresses were expected to develop. Following loss of crestal bone down to the most coronal thread (the final crestal bone configuration as observed in the animal study after 22 weeks of orthodontic loading<sup>20</sup>), the predicted maximum stress increased by about 20% (from 6.56 to 8.03 MPa) for the machined threaded design. In addition, while the maximum stress was predicted next to the most superior thread region, other local stress peaks were predicted next to the other thread positions along the implant length (Fig 9). The stress distribution at the depth of the most superior thread was very asymmetrical, with significantly lower stresses next to the surface opposite to the direction of the traction force (Fig 10).

For the porous-surfaced implant design, lower maximum stresses were predicted in the peri-implant bone in approximately the same locations as for the threaded implant design (Table 3 and Figs 6a and 6b). Maximum stresses of 4.02 MPa for the initial bone configuration (crestal bone to the top of the machined collar region of the implant), and minimal change (from 4.02 to 4.00 MPa) in the final bone con-

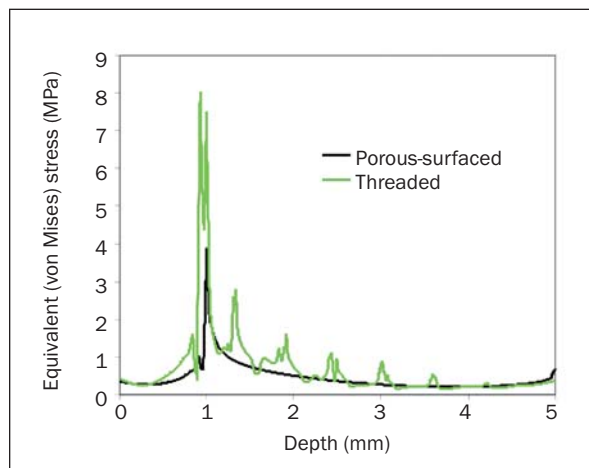
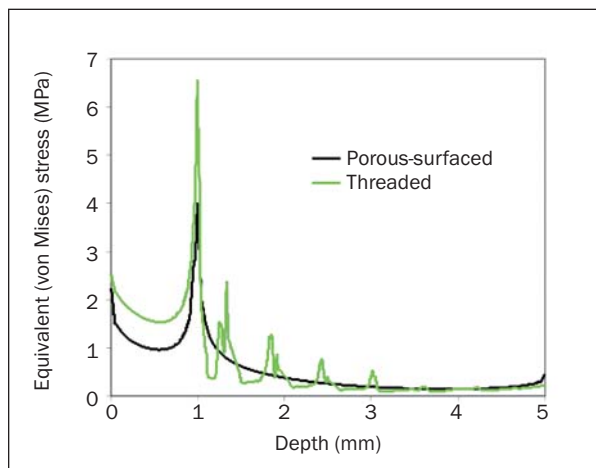


**Fig 9** Equivalent von Mises stress distribution inside the bone at the bone-implant interface for: (a) initial and (b) final bone geometry.

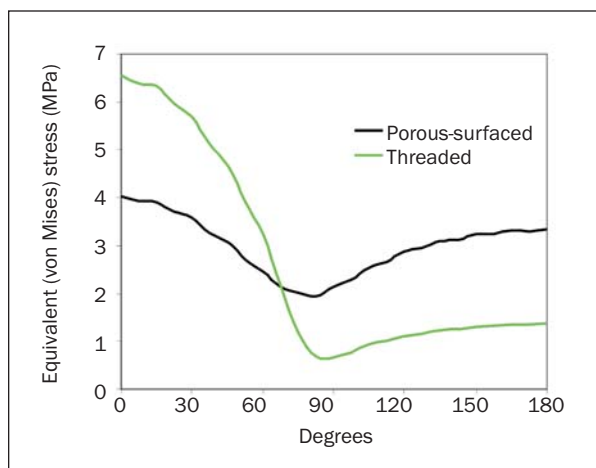


**Fig 10** Equivalent (von Mises) stress distribution inside the bone at the bone-implant interface at 1 mm below the bone surface in the circumferential direction for the initial bone position.  $\theta = 0$  degrees corresponds to the direction of orthodontic force application.

figuration model (crestal bone loss to the smooth-to-porous surface junction) were predicted. In addition, as seen in Fig 10, a more uniform distribution of stresses in the mesial-distal direction was predicted both for the starting and final crestal bone positions.

### FEA—Submodel

The results obtained for the submodel are shown in Fig 11. Since the submodel was used only to justify the use of the complete-bonding assumption, only 1 case (initial bone position with a maximum bone depth of 5 mm) in 1 location (where maximum values of bone stress/strain were predicted) was examined. The results showed that predicted values of maxi-

imum stress and stress contour patterns using the submodel were very similar to those predicted with the complete-bonding model. The maximum stress value at the buccal-lingual mid-plane section of the submodel also occurred at the superior zone of the porous-surfaced region of the implant-bone interface (4.49 MPa versus 4.02 MPa for the complete-bonding model). The small difference between the results obtained with the submodel and those obtained with the full model could be attributed to the use of different finite mesh elements and densities as well as approximation errors of the submodeling technique.

Figure 11 shows the von Mises stress distribution at 2 locations: along the interface length and along the circumference at the depth where these stresses reach their maximum values (1 mm below the initial bone surface for the complete-bonding “full” model and 0.978 mm below for the submodel). The results demonstrate that the refined stress field in the bone ingrowth region yields the same predicted stress pattern as that resulting from the use of the simpler complete bonding model, thereby justifying the use of the latter to represent the 3D mechanical interlock condition at the interface between the bone and the porous surface.

## DISCUSSION

As noted, differences in extent of crestal bone loss with the 2 implant designs studied were observed in the animal study that formed the basis for this 3D FE study.<sup>20,21</sup> The observed loss of bone from the initial position (at the top of the machined collar) down to the smooth-to-porous surface junction for porous-surfaced implants was identical to that reported in previous studies<sup>11–14</sup> and was attributed to under-

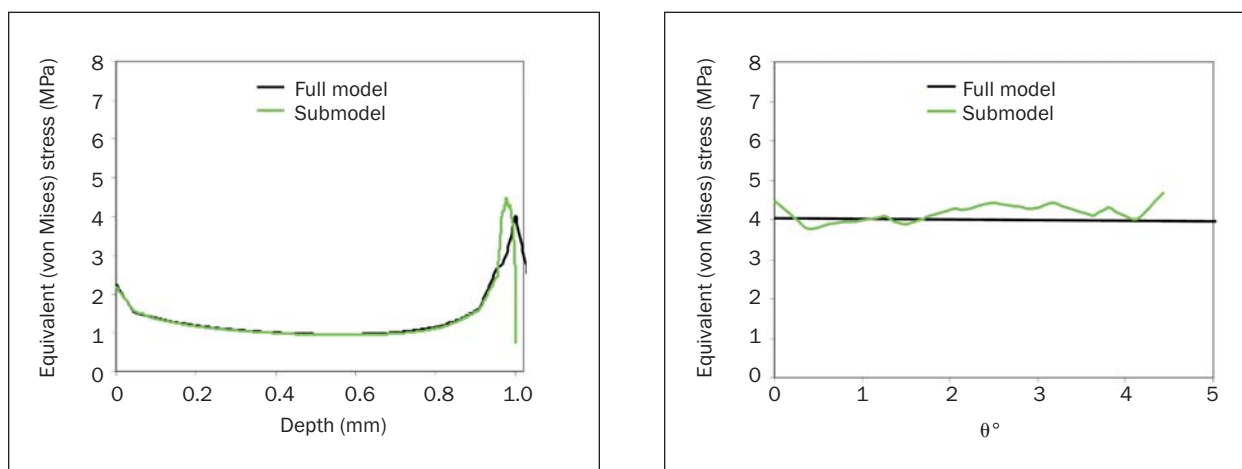


**Fig 11** Von Mises stress distribution at 2 locations: (a) along the interface length and (b) along the circumference at the depth where these stresses reach their maximum values (1 mm below the initial bone surface for the full model and 0.978 mm below for the submodel).

stressing of bone as a result of stress shielding and poor force transfer from implant to bone in the area of the smooth coronal portion of the implant,<sup>27,28</sup> although the contribution of “biologic width” accommodation<sup>29</sup> cannot be dismissed. In the present FE study, assuming virtual bone maintenance to the superior implant aspect and bone ingrowth into the porous-surfaced region (Fig 9a), lower stresses were predicted in bone located next to the smooth coronal region of the porous-surfaced implant, which supports the hypothesis that bone loss occurred in this region because of stress shielding. The higher stresses at the start of the porous-surfaced region suggest that this effect is lost and that bone maintenance will result in this region, as is the case. A similar change from lower to higher bone stresses was predicted with the threaded design, but peak stresses were almost twice as high next to the most coronal nonthreaded region of the implant compared with the porous-surfaced design. Apical to this region, much higher peak stresses were predicted for the threaded design. The maximum bone stress next to the most coronal thread was approximately 50% higher than that for a comparable position for the porous-surfaced design. Significantly higher local stresses were also predicted along the implant length in bone next to the tips of the threads. The differences in predicted peri-implant bone stress patterns along the implant length, assuming bone loss down to the beginning of the porous region for the porous-surfaced implants and to the beginning of the threaded portion of the implant for the screw-type implants, were even more dramatic (Fig 9b). In this case, the peak stresses next to the threaded implant were more than double those with the porous-surfaced design.

The stresses predicted to act within the peri-implant bone at the bone-implant interface and 1 mm below the initial crestal bone surface (the location of the most superior thread or the smooth-to-porous-surfaced junction) are shown in Fig 10. For both designs, the peak equivalent stresses occurred within bone in the direction of the imposed traction force. These stresses were primarily a result of compressive forces acting on bone at this location. Significantly greater maximum equivalent stresses were predicted for the threaded design at this location (approximately 6.5 versus 4.0 MPa). Next to the diametrically opposed implant surface, greater equivalent stresses were predicted with the porous-surfaced design as a consequence of the possible transfer of tensile forces across the bone-implant junction with this design. This is a consequence of the 3-dimensional mechanical interlock of bone and implant that is possible with bone ingrowth into the 3-dimensional porous network. As a result, the bone becomes tethered to the implant, allowing tensile force transfer across this interface. In contrast, the threaded design simply pulls away from the bone on the “tension” side of the implant, resulting in lower stressing of the peri-implant bone next to this surface. The net result is a more uniform distribution of stresses around the porous-surfaced implant; stress will be lower on the side in the direction of the traction force (the “compression” side) and higher on the diametrically opposed tension side. The total strain energy due to the orthodontic traction force is the same for both designs, but lower peak stresses develop in peri-implant bone next to the porous-surfaced implant.

These stresses can affect bone maintenance. Considering the FE model with bone present to the most superior aspect of the implant in the presence of

bone ingrowth into the porous surface region (porous-surfaced design) or direct bone apposition to the surface features of the threaded implant, higher peri-implant bone stresses and strains were predicted next to the threaded design. Sufficiently high strains will result in bone microfracture (strains  $> 4,000 \mu\epsilon^{30}$ ). The significantly higher stresses and strains predicted in bone next to the superior threads of the turned implants in comparison to those next to the porous-surfaced region support the hypothesis that this factor contributed to the observed differences in peri-implant bone appearance in the study by Oyonarte and associates.<sup>20</sup>

The predicted minimal change in maximum stress following loss of bone down to the smooth-to-porous surface junction with the sintered porous-surfaced implant (initial versus final bone position in Table 3) reflects the fact that very little force transfer occurs along the machined collar portion of the porous-surfaced implant. Whether bone is contacting this region has little effect in determining the stresses that develop in the bone next to the porous-surfaced region.

As already noted, the model used for the porous-surfaced implant, in which there was no incorporation of a "transition zone" with lower stiffness, represents the worst case for porous-surfaced implants in terms of the magnitude of predicted maximum stresses. Incorporation of a lower-stiffness transition zone (ie, a composite of bone and sintered titanium-alloy particles) would be expected to reduce the predicted maximum peri-implant bone stresses in the porous-surfaced implant model.

Other factors, such as disruption of the blood supply or peri-implant infection (peri-implantitis), can also promote crestal bone loss. However, it is unlikely that differences in vascularity occurred between the 2 implant designs, thereby discounting this as a factor contributing to the difference in the bone loss patterns observed. Peri-implant infection that could have resulted in marginal bone loss was not detected with any of the implants during the course of animal maintenance, thereby discounting this possibility. The reason for the observed difference in bone response with the 2 designs appears consistent with the biomechanical explanation suggested by the results of the FEA. A more favorable distribution of stresses within peri-implant bone next to the porous-surfaced implants supported the greater crestal bone retention with this design.

Avoidance of the initiation of crestal bone microfracture due to high local stress levels with machined threaded implants requires the use of longer implants. This, as reported recently,<sup>31</sup> would result in lower maximum equivalent stresses and strains. Bone quality also is expected to have a strong

effect, with lower-density cancellous peri-implant bone resulting in higher peri-implant stress and strain predictions for the cylindrical and screw-type implants studied by Tada and associates.<sup>31</sup> While cortical peri-implant bone was assumed in the present study, it is expected that the predicted differences in equivalent stresses in peri-implant bone for the 2 designs would also occur assuming cancellous peri-implant bone.

It is recognized that small, short implant devices are of considerable value in performing clinical orthodontic treatment. Traditional dental implants meant to replace teeth are often inappropriate for this application, as the patient may not be missing teeth in sites where the implants need to be placed to satisfy the orthodontist's anchorage requirements. Threaded mini-implants, which have been proposed for this purpose, must be used in long lengths (9 to 15 mm) to remain stable throughout the treatment. These nevertheless fail at a rate of  $> 10\%$ .<sup>9</sup> The present study has indicated the possible benefits of porous-surfaced orthodontic implants.

## CONCLUSIONS

The 3D FEA of a 3-N orthodontic traction force acting on relatively short (5 mm) threaded and porous-surfaced implants used as anchorage units predicts the development of maximum stresses in bone next to the coronal region of both designs. For the threaded implants, the peak stress occurs adjacent to the tip of the most coronal bone-contacting thread on the compression side of the implant. For the porous-surfaced implants, the peak stress is predicted to occur at the machined-to-porous surface junction but with both lower peak stresses and with a more uniform distribution of stresses around all aspects of the implant. Whereas progressive crestal bone loss is predicted to lead to much higher peak stresses in the remaining bone contacting the implant (again with the maximum next to the most coronal bone-interfacing thread), little change in peak stress is predicted with porous-surfaced implants. This difference in response is attributed to the very different interface bonding conditions both in reality and in the FE model, with the porous-surfaced design offering a means of efficient transfer of tensile as well as shear and compressive forces at the bone-implant junction. In contrast, with the machined threaded design, tensile and counter-rotation torsional shear forces cannot be effectively resisted.

## ACKNOWLEDGMENTS

Funding for this study was provided by a grant from the Canadian Institute for Health Research, while implants were provided by Innova LifeSciences as part of their contribution to an Ontario Research and Development Challenge Fund grant. The authors also wish to acknowledge the technical assistance of Ms Nancy Valiquette.

## REFERENCES

- Goodacre CJ, Brown DT, Roberts WE, Jeiroudi MT. Prosthodontic considerations when using implants for orthodontic anchorage. *J Prosthet Dent* 1997;77:162–170.
- Henry PJ, Singer S. Implant anchorage for the occlusal management of developmental defects in children: A preliminary report. *Pract Periodontics Aesthet Dent* 1999;11:699–706.
- Kanomi R. Mini-implant for orthodontic anchorage. *J Clin Orthod* 1997;31:763–767.
- Kyung SH, Hong SG, Park YC. Distalization of maxillary molars with a midpalatal miniscrew. *J Clin Orthod* 2003;37:22–26.
- Roberts WE, Smith RK, Ziberman Y, Mozsary PG, Smith RS. Osseous adaptation to continuous loading of rigid endosseous implants. *Am J Orthod* 1984;86:95–111.
- Akin-Nerzig N, Nergiz I, Schulz A, Arpak N, Niedermeier W. Reactions of peri-implant tissues to continuous loading of osseointegrated implants. *Am J Orthod Dentofacial Orthop* 1998;114:292–298.
- Majzoub Z, Finotti M, Miotti F, Giardino R, Aldini NN, Cordioli G. Bone response to orthodontic loading of endosseous implants in the rabbit calvaria: Early continuous distalizing forces. *Eur J Orthod* 1999;21:223–230.
- Wehrbein H, Glatzmaier J, Yildirim M. Orthodontic anchorage capacity of short titanium screw implants in the maxilla. An experimental study in the dog. *Clin Oral Implants Res* 1997;8:131–141.
- Cheng S-J, Tseng I-Y, Lee J-J, Kok S-H. A prospective study of risk factors associated with failure of mini-implants used for orthodontic anchorage. *Int J Oral Maxillofac Implants* 2004;19:100–106.
- Pilliar RM. Overview of surface variability of metallic endosseous dental implants: Textured and porous-surfaced designs. *Implant Dent* 1998;7:305–314.
- Deporter DA, Watson PA, Pharoah M, Todescan R, Tomlinson G. Ten-year results of a prospective study using porous-surfaced dental implants and a mandibular overdenture. *Clin Implants Dent Relat Res* 2002;4:183–189.
- Deporter DA, Pilliar RM, Todescan R, Watson PA, Pharoah M. Managing the posterior mandible of partially edentulous patients with short, porous-surfaced dental implants: Early data from a clinical trial. *Int J Oral Maxillofac Implants* 2001;16:653–658.
- Hagi D, Deporter DA, Pilliar RM, Arenovich T. A targeted review of study outcomes with short (7 mm or less) endosseous dental implants placed in partially edentulous patients. *J Periodontol* 2004;75:796–802.
- Deporter DA, Todescan R, Watson PA, Pharoah M, Pilliar RM, Tomlinson G. A prospective human clinical trial of Endopore dental implants in restoring partially edentulous maxilla using fixed prostheses. *Int J Oral Maxillofac Implants* 2001;16:527–536.
- Pilliar RM. Processing and properties of endosseous dental implant surfaces: Design for increased osseointegration potential. *Oral Health* 2000;(August): 51–58.
- Dziedic DM. Effects of Implant Surface Topography on Osteoconduction [thesis]. Toronto: University of Toronto, 1994.
- Simmons CA, Valiquette N, Pilliar RM. Osseointegration of sintered porous-surfaced and plasma-spray coated implants: An animal model study of early post-implantation healing response and mechanical stability. *J Biomed Mater Res* 1999;47:127–138.
- Carter DR, Beaupre GS, Giori NJ, Helms JA. Mechanobiology of skeletal regeneration. *Clin Orthop* 1998;355(suppl):S41–S45.
- Simmons CA, Meguid SA, Pilliar RM. Mechanical regulation of localized and appositional bone formation around bone-interfacing implants. *J Biomed Mater Res* 2001;55:63–71.
- Oyonarte R, Deporter D, Pilliar RM, Woodside DG. Peri-implant bone response to orthodontic loading: Part 1. The effects of implant surface design, a histomorphometric study. *Am J Orthod Dentofacial Orthop* 2005;128:173–181.
- Oyonarte R, Deporter D, Pilliar RM, Woodside DG. Peri-implant bone response to orthodontic loading: Part 2. Implant surface geometry and its impact on regional bone remodeling. *Am J Orthod Dentofacial Orthop* 2005;128:182–189.
- Van Oosterwyck H, Duyck J, Vander Sloten J, Van der Perre G, Naert I. Peri-implant bone tissue strains in cases of dehiscence: A finite element study. *Clin Oral Implants Res* 2002;13:327–333.
- ANSYS Structural Analysis Guide, Version 5.6 and higher, ANSYS Online Help, SAS [unpublished work, 2003]. Available at: <http://www.oulu.fi/atkk/tpalv/unix/ansys6.1/content/index.html>
- ANSYS User's Manual, ver. 5.6-8.0. Cary, NC: SAS, 2000–2004.
- Dammak M, Shirazi-Adl M, Schwartz Jr M, Gustavson L. Friction properties at the bone-metal interface: Comparison of four different porous metal surfaces. *J Biomechanics* 1997;35:329–336.
- Vaillancourt H, Pilliar RM, McCammond D. Finite element analysis of crestal bone loss around porous-coated dental implants. *J Appl Biomater* 1995;6:267–282.
- Pilliar RM, Deporter DA, Watson PA, et al. The effect of partial coating with hydroxyapatite on bone remodeling in relation to porous-coated titanium-alloy dental implants in the dog. *J Dent Res* 1991;70:1338–1345.
- Al-Sayyed A, Deporter DA, Pilliar RM, et al. Predictable crestal bone remodelling around two porous-coated titanium alloy dental implant designs. A radiographic study in dogs. *Clin Oral Implants Res* 1994;5:131–141.
- Abrahamsson I, Berglundh T, Wennstrom J, Lindhe J. The peri-implant hard and soft tissues at different implant systems. A comparative study in the dog. *Clin Oral Implants Res* 1996;7:212–219.
- Roberts WE. Fundamental principles of bone physiology, metabolism and loading. In: Naert I, van Steenberghe D, Worthington P (eds). *Osseointegration in Oral Rehabilitation: An Introductory Textbook*. London: Quintessence, 1993:157–180.
- Tada S, Stegaroiu R, Kitamura E, Miyakawa O, Kusakari H. Influence of implant design and bone quality on stress/strain distribution in bone around implants: A 3-dimensional finite element analysis. *Int J Oral Maxillofac Implants* 2001;16:527–536.